Magnetic Resonance Force Microscopy and the spin bath : towards single-spin massive-resonator entanglement and the spoiling influence of the spin bath

Voogd, J.M. de

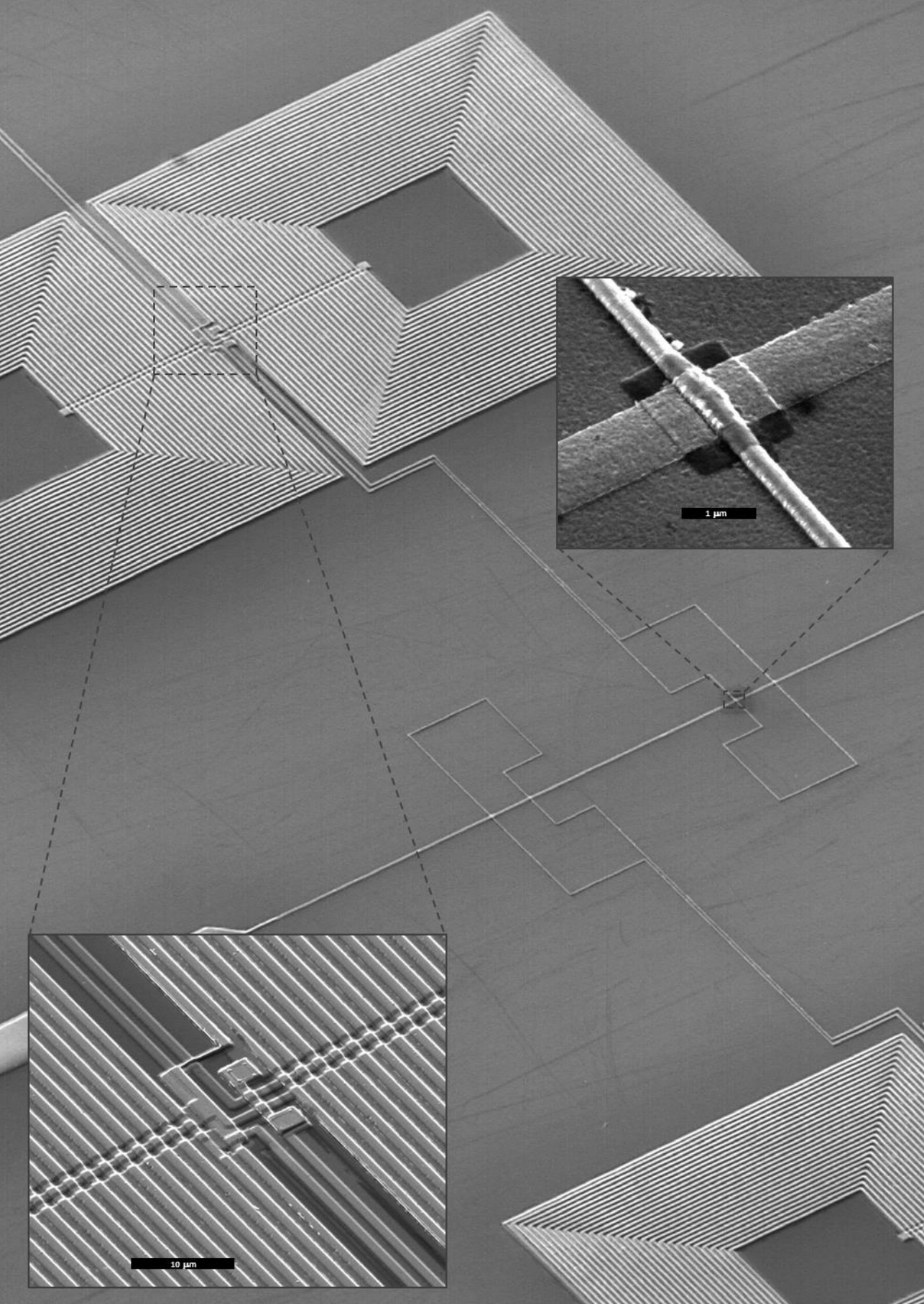
1 µm
10 µm

6 *Techniques and instrumentation*

Researchers sometimes refer to MRFM as the 'crosstalk microscope' when the analysis of obtained signals drive them crazy. The reason for this is on the one hand the supreme sensitivity, and on the other hand the extreme technical criteria and operational conditions for an MRFM apparatus. For example: to show the required sensitivity, consider the thermal force noise amplitude spectral density $\sqrt{S_F} = \sqrt{4k_B T \frac{k}{\omega\, Q}}$ which is[1] about 1.3 aN/$\sqrt{\text{Hz}}$. This is even lower when the experiment cools to temperatures of 10 mK and the cantilever reaches Q-factors exceeding 100 000, numbers that are actually reached in our setup, leading to an ultimate force noise of about 0.1 aN/$\sqrt{\text{Hz}}$. A popular analogy illustrating this tiny number is the gravitational force between a mosquito and a human body at a distance of 365 m.[2] Note however that, for reasons explained in Ch. 2, the Q-factor can become much lower close to the sample and that the vibrational noise can prevent the mechanical mode from cooling to 10 mK. This exemplifies the extreme conditions at which the MRFM should operate and the as yet seemingly impossible and mutually conflicting criteria the setup should meet.

[1] Using typical parameters from our experiments: $T \sim 100$ mK, $k = 50$ μN/m, $\frac{\omega}{2\pi} = 2750$ Hz, and $Q = 10\,000$.

[2] A consistent analogy should remark that the mass of the mosquito flickers on and off at the resonance frequency.

This chapter gives a brief account of some of the things that we conceived, designed, or further developed for the research done in Chs. 3 and 4.[3] For these experiments we also used techniques that are reused or copied from previous experiments without improving them significantly, such as

[3] Upon finishing this thesis many of these things are still in use, or used for other research.

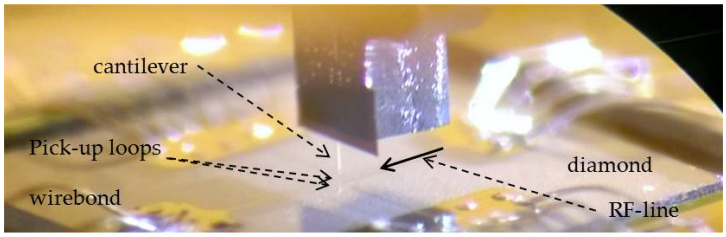

Figure 6.1: In situ image of the diamond sample with wire-bonded RF-line (emphasized with the solid arrow) and two pick-up loops (to small to see). The tiny bright beam beneath the silicon chip is a projection of the cantilever.

vibration isolation. Therefore they are not described in this chapter, but left in the theses of predecessors.[4,5,6]
In this chapter we will for didactic reasons start describing the system at the heart of the experiment, and from there working our way out.

[4] Usenko 2012
[5] Wijts 2013
[6] Haan 2016

6.1 Sample

It is the defects in diamond that we wanted to measure. The defects can be seen as small magnets (spins) that interact with the magnetic tip of the cantilever which is suspended just above the sample. The photo in Fig. 6.1 shows the cantilever positioned above the diamond substrate just before cooling down the experiment. When the spins rotate, the magnetic tip starts to oscillate and vice versa. Another way of rotating the spins is resonantly exciting them with a fast oscillating magnetic field (RF-field). The needed frequency depends on the magnetic field and the type of spin. The ones that we are interested in need to be excited between 0.1 and 5 GHz considering our conditions, see for more information Secs. 4.4 and 4.5. In our experiment, the larger the amplitude of the RF-field, the more accurate the response of the spin. Conventional magnetic resonance experiments use antennas to rotate the spins because antennas can accumulate the incoming RF-power and thus create large magnetic fields. In our experiments this is not an option as antennas are quite narrow banded and cannot easily be tuned to other

frequencies when cooled down to temperatures of 10 mK. For MRFM there are three reasonable options: 1) use an antenna and apply an external magnetic field to tune the frequency of the spins, 2) use an antenna and move the magnetic tip at the end of the cantilever to get the spins into the resonance slice, or 3) don't use an antenna but fabricate a wideband microstripline on top of the sample and only work with spins close to the line.

In our setup it is really difficult to apply an external field because we read out the motion of the cantilever using a SQUID, see Sec. 6.3, which is extremely sensitive to magnetic fields. We have tried this, but until now the SQUID became unstable, or the SQUID's noise-floor was dramatically increased.[7]

[7] Waarde 2016

The second option is very hard as one relies even more on the reliability of nanopositioning. The actuation at ultralow temperatures and its problems are described in Sec. 6.5. Another drawback is the trade-off between maximal depth of the resonance slice into the sample and the sensitivity[8] when designing the antenna's resonance frequency.

[8] Having the resonance slice closer to the tip implies a higher gradient which in turn implies better sensitivity.

This leaves open the third option. For the microstrip line we use superconducting wires as they have minimal dissipation. The thickness and width of the wire is a trade-off between heating[9] and how close the magnetic tip can approach. Wijts[10] has shown that superconducting wires cause significant repulsion due to the Meissner effect.

[9] Besides dielectric losses, superconductors still dissipate RF-currents, presumably due to moving of trapped flux quanta.

[10] Wijts 2013

Theoretically, the characteristic impedance of the microstrip, or more general 'waveguide', should be tuned as closely as possible to the characteristic impedance of the RF-power supply lines in the setup which is 50 Ω. However, let us assume a reasonable phase velocity of $\sim \frac{1}{2}c$,[11] then the wavelength is 50 mm at a frequency of 3 GHz. If the length of the unmatched part of the waveguide stays far below 50 mm, say $\sim$ 5 mm, then the transmitted wave is much larger than the reflected part[12] so we may assume that almost all RF-power arriving at the sample will be transmitted and thus will cre-

[11] c is the speed of light.

[12] Pozar 2011

ate an oscillating magnetic field in the sample.

THE MOVEMENT OF THE CANTILEVER needs to be detected as it encodes the information about the interacting spins. Conventional MRFM uses laser interferometry which can heat up the cantilever due to absorption and is limited in sensitivity due to the shot noise of a laser. Therefore we detect the movement of the magnetic tip in a different way: we measure the flux difference that is generated by the tip in a small superconducting pick-up loop. On our small diamond samples the fabrication is already difficult enough to fabricate a good single layer structure, however in the future the design of the pick-up loop could be much improved if we could go to multi-layer fabrication.[13] The general pattern as shown in Fig. 6.2, can also be used on other samples and is optimized for any of the three possible tip-magnetization directions.

THE ACTUAL DIAMOND SAMPLE is $2.6 \times 2.6 \times 0.3$ mm^3 which is an inconveniently small size to handle. Therefore we glued the diamond into the middle of a silicon carrier with either rubber cement[14] or wax.[15] The wax was easier to use as it becomes liquid at $\sim 60°C$, is very stiff at ambient temperatures, and, the process is reversible. A piece of metal of the same thickness as the sample is glued on all sides to prevent the resist from piling up at the edge of the diamond.
We used the following recipe:

- Spincoat copolymer MMA EL11 (thickness $\sim$ 610 nm) @4000 RPM, bake 80 s @150 °C.
- Spincoat PMMA A4 (thickness $\sim$ 190 nm) @4000 RPM, bake 30 min. @120 °C in a vacuum oven.
- Spincoat PSSA[16] @4000 RPM, bake 5 min. 90 °C in vacuum oven.
- Sputter 15 nm of chrome.
- Expose 1050 μC/cm^2 [17] @100 kV.

[13] We tried this on silicon and the result is promising, but we need more testing. See also Sec. 6.3

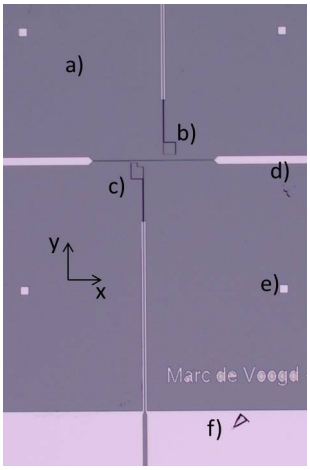

Figure 6.2: Optical microscope photo of diamond sample. This general single layer layout can be used on any sample as the pick-up loops are optimized for any magnetization direction and the added markers make it possible to position another layer or sample. a) Diamond sample, b) simple pick-up loop, c) pick-up loop with extra corner for a tip magnetized in the $y-$direction, d) RF-line, e) marker, f) bonding pad.

[14] Marubu Fixogum

[15] SPI supplies, crystalbond 509 #5110-AB

[16] Poly(4-styrenesulfonic acid) solution in water. This layer makes a chrome etch unnecessary as PSSA can be removed in water: the chemical chrome etch leaves residues when removing complete layers.

[17] This is the base dose; proximity effect correction (PEC) calculates the best dose for each area of the pattern.

- Sample in water for $\sim$ 1 min, then intensively but gently rinsing.
- *(if necessary)* When chrome is not completely removed do a quick chemical chrome etch in CE no1.
- Develop 40s in MIBK 1:3 IPA[18].
- Dissolve developer 60 s in IPA and dry gently with N_2.
- *(if necessary)* Just before applying NbTiN, do very soft oxygen plasma etch (100 W, 30 s) to enhance sticking.
- Sputter 250 nm NbTiN.
- *From this part it becomes difficult to not drop the diamond as it comes off the carrier!* Lift-off: 15 min. in acetone, then while (!) rinsing with acetone, move the diamond to a cleaner beaker with acetone and leave it overnight.
- After one night, while rinsing with IPA, move the sample to a beaker with IPA, do ultrasonic cleaning for few minutes, rinse with IPA, then rinse with water and dry with N_2.

[18] MIBK is short for 4-methyl-pentan-2-on, and IPA stands for iso-propanol but is officially known as propan-2-ol.

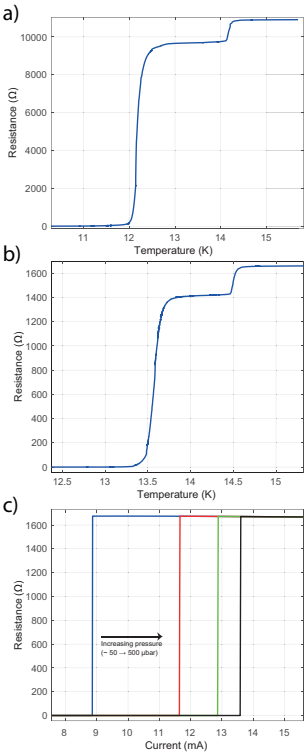

Figure 6.3: The superconducting lines are tested in a vacuum chamber inside a helium dewar. a,b) The resistance as function of temperature for the pick-up loop a) and RF-wire b). The steps can be ascribed do to impurities in small lines of the structure due to the resist present during the NbTiN deposition process. The effect is larger in a) than b) since the pick-up loop has smaller structures than the RF-wire. c) Measurement of the critical current of the RF-wire, determining the maximal B_1-field strength that can be applied.

Testing the sample was done in a helium dewar. A newly designed helium dipstick made it possible to quickly cool the sample under the expected superconducting temperature of 15 K. The sample holder is equipped with a heater and a thermometer. Furthermore, each superconducting bonding pad was wirebonded to two electrodes such that a four point measurements could be conducted. The results are given in Fig. 6.3.

6.2 Cantilever

An ultrasoft silicon cantilever[19] with dimensions 150

[19] Chui et al. 2003

μm long, 4 μm wide, 100 nm thick is clamped upon a HV-compatible nanomanipulator that can work inside an electron microscope. On the other side of the manipulator we sticked a carbon tape covered with NdFeB powder which consists of nice spherical balls ranging from 1 μm to 100 μm in diameter. After aiming for a particle of about 3 μm diameter size,[20] we glued a particle of 2.99 μm onto the cantilever tip.

[20] Smaller NdFeB magnets tend to loose their remanence field, larger particles have lower field gradients.

It is possible to measure the resonance frequency of the new magnetic force sensor inside the electron microscope. The spring constant can be obtained by measuring the resonance frequency before and after attaching the magnet.[21] The final spring constant and frequency are named k_{sem} and f_{sem} respectively. If due to environmental conditions inside the cryostat the frequency changes to f_0, the new spring constant k_0 can be calculated by

[21] Wijts 2013

$$k_0 = \sqrt{\frac{f_0}{f_{sem}}} k_{sem}. \tag{6.1}$$

At cryogenic temperatures and no influence from the sample we obtained $f_0 = 2748.5$ Hz and $k_0 = 48.6$ μN.

6.3 SQUID

To MEASURE THE FLUX generated by the moving magnet on the MRFM-tip, we use a SQUID. This Josephson junction based device only works at cryogenic temperatures as it uses superconductivity principles.[22] The typical flux noise floor is about 1 $\mu\Phi_0/\sqrt{\text{Hz}} \approx 2 \cdot 10^{-21}$ Wb$/\sqrt{\text{Hz}}$. The other two important parameters are the input inductance L_{in} and mutual inductance M between the input coil and the SQUID loop as shown in Fig. 6.4a. It is suggested[23] that the Johnson noise in the internal currents through the Josephson junctions is so small that it can be ignored, meaning there is no backaction from the SQUID unto the cantilever.

[22] When we talk about SQUIDs, we mean DC-SQUIDs.

[23] Quantum Design 2001

THE FLUX ϕ_{in} generated by the magnetic tip depends on the movement of the cantilever and the pick-up loop geometry. ϕ_{in} does not depend on the inductances and thus can be seen as constant in this section. The current generated by ϕ_{in} does depend on the total inductance L_{tot} of the loop, thus

$$\frac{\phi_{out}}{\phi_{in}} = \frac{M}{L_{tot}}, \tag{6.2}$$

where ϕ_{out} is the flux that is transferred to the SQUID. As can be seen in Fig. 6.4, $L_{tot} = L_{in} + L_{pul} + L_{par}$, where L_{pul} is the inductance of the pick-up loop and L_{par} the parasitic inductance.[24] Taking into account typical values of M and L_{tot}, we only reach percentages of less than 1% of the flux ϕ_{in} that is transferred to the SQUID ϕ_{out}.

This can be improved by using transformers to match the inductances. The incoming versus outgoing flux ratio is given by[23]

$$\frac{\phi_{out}}{\phi_{in}} = \frac{MM_{12}}{L_{pr}L_{se} + M_{12}^2} \qquad \text{for Fig. 6.4b, and} \tag{6.3}$$

$$\frac{\phi_{out}}{\phi_{in}} = \frac{MM_{12}M_{34}}{(L_{se}L_{te} + M_{34}^2)L_{pr} + L_{te}M_{12}^2} \qquad \text{for Fig. 6.4c.} \tag{6.4}$$

It is now easy to calculate an optimal L_1 and L_2 given a certain coupling factor. For superconducting transformers we believe we can achieve inductive coupling factors of ~ 0.9. This would make the maximal flux input $\sim 50\%$ if we could fabricate the transformers with the optimal values for L_1 and L_2. However, in practice we were bound by the available transformers whose L_1 is too small and L_2 too large. Hence the flux coupling was $0.5 - 5\%$, depending on the SQUID type used.[25]

A second transformer as shown in Fig. 6.4c could easily boost the flux ratio to $10 - 15\%$, or more if the transformer is made on-chip, considering the absence of parasitic inductances in the first loop. We fabricated an on-chip transformer on silicon as a proof of principle that we can fabricate it at the desired dimensions and without damaging the sample surface, see Fig. 6.5. The double metal-layer fabrication has more advan-

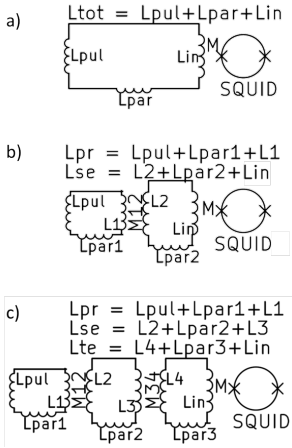

Figure 6.4: Impedance matching becomes inductance matching for circuits without resistances (due to superconductivity) and capacitances (neglectable due to low impedance circuits). L stands for the self inductance of the coils and M for the mutual inductances. The flux comes into the circuit via the small L_{pul}, usually around 10 pH, and needs to be transferred to the SQUID via the relatively large L_{in}, usually > 100 nH and < 10 µH.

[24] For example: L_{par} can come from wirebonds, other wiring, or even superconducting filters.

[25] The value of M and L_{in} are determined by the SQUID type.

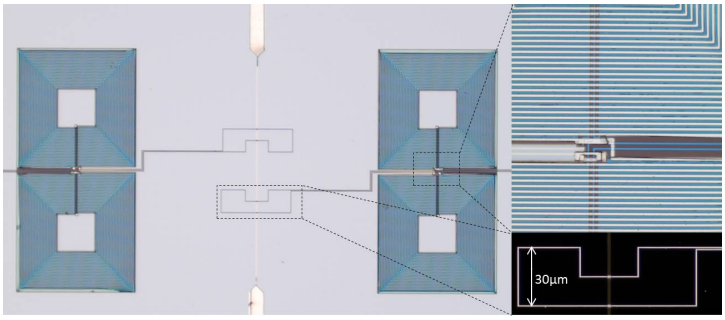

Figure 6.5: NbTiN structures fabricated on silicon. The vertical line is the RF-wire, separated from the overlaying U-shaped pick-up loops by 3×3 μm^2 squares of SiN as can be seen in the right-bottom inset. The signal generated inside the pick-up loop is up converted onto higher impedances by means of a gradiometric transformer. The nontrivial connection in the center of the transformers enables fabrication of the device in only two metal (NbTiN) layers and one insulating spacer (SiN). The lines inside the transformer and the RF-line have a width of 1 μm and the pick-up loop has a linewidth of 0.4 μm

tages such as minimization of the mutual inductance between pick-up loop and RF-line. The improvement of the flux ratio is expected to be about a factor of ten higher compared to the current setup. Testing and implementing of this design is left for successive research projects.

6.4 *Anneal-o-tron*

The wirebonds to the structures on the sample need to be superconducting. Any resistance will decay the signal and/or heat up the sample. For many experiments we used aluminum wirebonds only, since we would run them solely below 1 K. For some experiments, like testing the RF-line currents, it is advantageous to use materials with a T_c higher than liquid helium temperatures. The problems with Niobium wirebonds are that the material is very stiff due to some impurities, and it has a thick oxide layer. This problem can be made easier by annealing the material for a short time close to its melting temperature. Annealing too long will stiffen the wire again; an anneal time of ~ 5 min. seems to produce the optimal softness.

We invented a system to do this annealing quickly. The system can be mounted directly on top of a pump station. This 'anneal-o-tron' is a simple vacuum pipe with viewports

halfway. The main part of this system is the vacuum insert consisting of three metal rods with two clamps each. The clamps are very fine machined as they can tightly grab a 25 μm diameter wire without breaking it. The anneal-o-tron can be pumped down to 10^{-5} mbar within 15 min. The annealing itself takes about $5-6$ minutes. For the first wire one might try to find the current at which the wire breaks, for us around 0.2 A. A bit less current, ~ 0.18 A, should produce a good annealing temperature, see Fig. 6.6.

The bonding itself might still be hard because of the niobium oxide layer. Considering the limited amount of wire, we position the wire with a tweezer and stamp it onto the bonding pad with a waffle foot wedge[26] using an ultrasonic wirebonder system. The waffle foot makes it possible to apply a lot of force without breaking the wire and hence ultrasonically welding through the oxide layer.

Figure 6.6: *top*: anneal-o-tron, *middle*: clamps holding a 25 μm diameter wire, *bottom*: annealing of niobium wire.

[26] 7145W-M-0055-L-M-A, waffle foot wedge *from* Small Precision Tools

6.5 Nanopositioning

One of the hardest parts of an MRFM microscope is the maneuvering of the tip with respect to the sample while the experiment is cooled to temperatures below 1 K. A short design brief for such a positioning system considering only the most important aspects includes:

1. (sub) nanometer positioning with at least 1 mm travel range in all three dimensions,
2. reliable working at ultra low temperatures,
3. maximal dissipation < 1 μW,
4. stiffness of mechanical loop > 3 kHz,
5. nonmagnetic, heat conducting materials,
6. magnetic-field shielding outerbody,
7. absolute position readout with nanometer precision.

All practical solutions to the individual requirements, except for the last one, are conflicting with at least one other requirement. For example, copper is a nonmagnetic, very well heat conducting material and is a practical solution; meaning it is relatively cheap and easy to machine. However, the material is not stiff and very heavy, thereby decreasing the stiffness of the mechanical loop. From a scientist's viewpoint, a better choice would be beryllium with the outerbody covered with a layer of lead,[27] which would, at least partially, satisfy requirements $4-6$, however machining this is an engineer's death wish. In our last design we have chosen an aluminum body with a thick gold layer to cool the motor body when the aluminum is below its superconducting temperature.[28] Some manufacturer parts are used as is and they are mainly made of titanium and stainless steel. This is unfortunate as titanium has a superconducting transition within the measurement temperature range, and stainless steel is a little bit magnetic and has poor heat conducting properties. These compromises had to be taken in view of time constraints.

Due to requirements 3 and 6, motors that create large magnetic fields are not suitable. Considering the low temperature, low vibrational environment, we are naturally left with piezoelectric driven motors. Piezos are not free of problems either, however, as their thermal expansion differs from most other materials and their travel range lowers by a factor five when cooled below $\sim$ 80 K. This means that piezowalking motors need extremely fine machining to overcome imperfection with respect to the reduced travel range.[29] It is therefore much simpler to use a stick-slip based design, although this probably violates requirement 3. Commonly used piezostacks, that have larger travelranges than single piezos, have low resonance frequencies and therefore it is best to find a design where these piezos are not part of the mechanical loop.

A WELL ESTABLISHED DESIGN and a trade-off between most requirements is the tripod design as schematically shown in

[27] Lead is superconducting below 7.19 K.

[28] Pure aluminum has a critical temperature of 1.2 K, but aluminum often used for machining has a critical temperature just below 1 K.

[29] The piezowalker is further discussed at the end of this section.

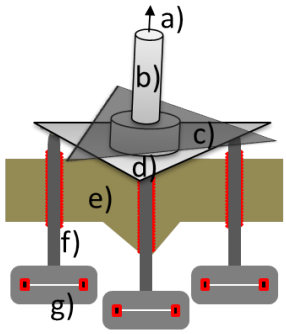

Figure 6.7: Schematic of tripod motor design. a) MRFM probe, b) tower to convert rotation into displacement, c) (dark grey triangle) leaf spring to fix horizontal position of tower base, corners of leaf spring are fixed to motor body, (not shown), d) (light grey triangle) tower base which is moved by spindles, e) motor body, f) spindle, g) piezo knob.

Fig. 6.7. The three parallel mounted linear motors move the triangular base of the tower, thereby wiggling the tower with the cantilever on top in three directions. The linear motors are spindles which are driven by JPE's piezo knobs[30] that move using the inertia of the heavy ring around the knob. The piezos that hold the ring can create this inertia. The stick-slip effect takes place between the spindles and nuts, and between the tips of the spindles and the feet of the tower. The knob itself is completely outside the mechanical loop of the cantilever to the sample, see Fig.6.8. The power each motor dissipates is about 1 mW, generated in a brief slip moment in the piezos and also at the contact surface between spindle and nut. To make the cooling faster than in earlier designs, where most of the heat flow goes through the motor body, we connected copper strips between the nuts and the cryostat's mixing chamber plate.

[30] Cryo Linear Actuator, piezo knobs, *from* Janssen Precision Engineering

OTHER THINGS we have done to cool the experiment efficiently involves a flame annealed silver strip providing an excellent heat conductance from sample holder and cantilever to the mixing chamber plate. The strip is isolated from other parts of the experiment. A heater is mounted on the strip which can heat the sample and cantilever homogeneously or can be used to keep the temperature constant. The combination of minimal heat capacitance for the sample and cantilever holders and a fast thermometer[31] mounted on the sample holder makes heating the sample to any specific temperature between 10 mK and 1 K a matter of seconds. Also cooling to any temperature can be done well within a minute, provided that the base temperature of the cryostat is at least about 15 mK below the required temperature.

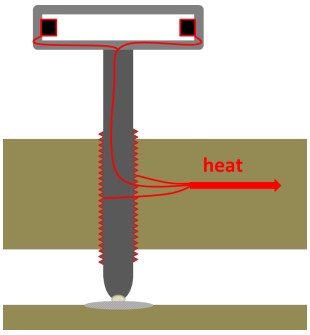

Figure 6.8: Cross section of spindle and piezo knob.

[31] Custom thermometer *from* HDL

FOR THE POSITION READOUT with nanometer precision we considered two options. The first option is interferometry. Despite the subnanometer precision, there are two problems with this technique: it can heat up the system and, more im-

portantly, it is difficult to measure absolute distances on the micrometer to millimeter scale. We choose to use capacitance readout. The advantages are that the readout itself does not dissipate energy, the position readout is absolute, and it is relatively easy to fabricate the sensors, such that you can make them for every custom application. In fact, for conducting probes one can even use the capacitance between probe and sample as a measure for tip-sample distance. This is further explored in Sec. 7.2, that also explains the details of the principle of capacitance measurements.

We used the capacitance readout to determine the three dimensional position of the probe with respect to the sample. The capacitor was designed as a three-segmented ring to which a variational voltage is applied, see Fig. 6.9. The orientation of the receiver ring, mounted at the bottom of the tower, can be easily measured, and thereby the orientation of the tower and thus the position of the probe. The parallel plate capacitance is

$$C = \frac{\epsilon_0 a}{d}, \tag{6.5}$$

with ϵ_0 the permitivity in vacuum, a approximately the surface of the overlay of the capacitor plates and d the distance between the capacitance plates. As to first order the effective surface of the capacitor plates does not change when the spindles move to length L, and since $L \propto d$, we can write a general linear dependency

$$\begin{pmatrix} L_1 \\ L_2 \\ L_3 \end{pmatrix} = A \begin{pmatrix} 1/C_1 \\ 1/C_2 \\ 1/C_3 \\ 1 \end{pmatrix}, \tag{6.6}$$

where A now is a 3×4 matrix, with the first three columns converting reciprocal capacitance to length and the last column is used to set an arbitrary origin in the L-basis. The conversion from L-basis to a Cartesian basis for the probe's position can now be calculated. The only thing that is needed

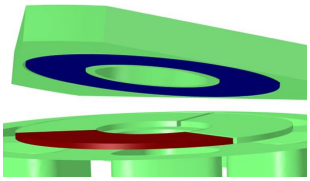

Figure 6.9: Capacitance sensors for 3D-position readout drawn in COMSOL. The three segments at the lower part (one of which is red) are sequentially activated by a 1 kHz voltage. This can be measured with the blue receiver plate due to the mutual capacitance. The capacitance of each of the three segments to the blue plate determines the orientation of the upper part (which is the foot of the tower, not drawn here). The tilt of the upper part is much less in reality.

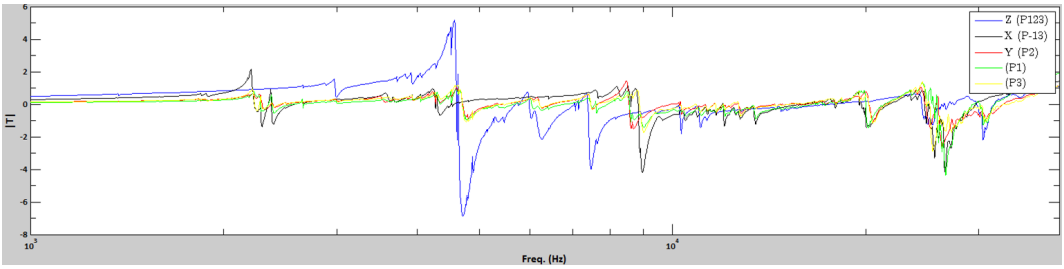

Figure 6.10: Correction to transferfunction of finestage piezos compared to theoretical piezo transferfunction, measured when actuated in Cartesian directions. Here we have chosen z to be a linear combination of all three piezo's (P1+P2+P3), x the difference betweeen two piezo's (P3-P1), and y is proportional to a single piezo (P2).

to be done now is finding A. Each L is the height of a hyperplane above a three dimensional reciprocal capacitance plane. Each row of A can then easily be calculated by fitting the hyperplane through a set of calibration points. For the j^{th} row of A, the coefficients can be calculated by

$$\begin{pmatrix} A_{j1} \\ A_{j2} \\ A_{j3} \\ A_{j4} \end{pmatrix} = \left[\sum_{i=1}^{n} \begin{pmatrix} \left(\frac{1}{C_{1i}}\right)^2 & \frac{1}{C_{1i}C_{2i}} & \frac{1}{C_{1i}C_{3i}} & \frac{1}{C_{1i}} \\ \frac{1}{C_{1i}C_{2i}} & \left(\frac{1}{C_{2i}}\right)^2 & \frac{1}{C_{2i}C_{3i}} & \frac{1}{C_{2i}} \\ \frac{1}{C_{1i}C_{3i}} & \frac{1}{C_{2i}C_{3i}} & \left(\frac{1}{C_{3i}}\right)^2 & \frac{1}{C_{3i}} \\ \frac{1}{C_{1i}} & \frac{1}{C_{2i}} & \frac{1}{C_{3i}} & 1 \end{pmatrix} \right]^{-1} \left[\sum_{i=1}^{n} \begin{pmatrix} \frac{1}{C_{1i}L_{ji}} \\ \frac{1}{C_{2i}L_{ji}} \\ \frac{1}{C_{3i}L_{ji}} \\ \frac{1}{L_{ji}} \end{pmatrix} \right], \quad (6.7)$$

where $\left(\frac{1}{C_{1i}}, \frac{1}{C_{2i}}, \frac{1}{C_{3i}}, L_{ji}\right)$ is one of n calibration points. There should be more than 4 independent[32] points for each j with a spread much larger than any measurement errors. This method automatically minimizes the summed square errors of the data points with respect to the hyperplane in the L-direction.[33]

Once A is known it is straightforward to measure the three capacitances,[34] to calculate L, and from there the tip position. In full operational conditions, the absolute resolution was 10 to 100 nanometers for the tip position in the Cartesian basis.[35]

THE RESONANCES in the mechanical loop are determined by the linear response of small piezo elements that are placed at the end of the spindles. The linear response is derived from an electrical impedance measurement. The result is shown in Fig. 6.10. The largest resonance at 4.5 kHz is certainly higher than the cantilever frequency of about 3 kHz, however small peaks still appear around the cantilever frequency. This is

[32] Independent meaning that one point does not scale to another by multiplication by a scalar (plus offset for L).

[33] JPE Precision Point 2013

[34] For which we use an automated capacitance bridge: AH2550 *from* Andeen-Hagerling.

[35] Depending on the orientation of the tower. In test situations the resolution was better, however capacitance measurements are very sensitive to ground loops and noise currents, inevitable in large set-ups.

what we also noticed when cooled to milliKelvin temperatures: these small peaks can drive the cantilever if their resonances overlap a bit. We can tune the cantilever's frequency a little bit by positioning it close to the superconducting RF-line, and thereby move the cantilever's frequency to cleaner parts of the spectrum.

To conclude the current design, we review requirements $1-7$. We have satisfied points 1 and 7 well enough for the experiments in Chs. 3, 4, and 7.[36] The trade-offs in the design led to only partially meeting requirements $3-6$ which was fine for now, but might need other solutions in the near future. The most difficult requirement, however, turned out to be 2: When the system is cooled down after thoroughly cleaning the spindles, then the motor usually does work only for the first hundred of microns of movement. Suddenly a spindle can get stuck. This is something we have encountered in many designs and we have not been able to determine the exact problem. Despite changing geometries, materials, piezo knobs and lubricators; the reliability is still a large issue.

[36] Especially the absolute position readout (point 7) is an important feature that also led to understanding the tip-sample capacitance in scanning probe microscopes, as published as Voogd et al. 2017a (Ch. 7).

Meanwhile we have gestated many piezowalker designs. The piezowalker consists of a piezo construction that makes a contact with the slider, shifts the slider, then retracts, returns to its starting position, and comes into contact again to set the next step. The design does not depend on fine-tuning of forces to overcome friction forces like in stick-slip mechanisms and is therefore radically different. Also, larger forces might be applied that can solve reliability problems as well as satisfy the other requirements generously. However, this is only possible if the tolerances on the material properties are tight enough and the machining can be done with sub micrometer precision, limited by the range of the piezos. The largest problem is the difference in thermal expansion of materials and the reduction of the piezo's travel range when

going to low temperatures. In close collaboration with LSI B.V., we developed an tested new designs. We made serious progress as we tested the motors thoroughly in liquid helium to measure the crimp, hysteresis, and reliability. Home made capacitance sensor were used to determine the differences in crimp between various parts with $\sim$ 50 nm precision. This led to a promising new design, which hopefully will provide a solution for low temperature MRFM and bring us a step closer to a commercial MRFM.[37]

[37] Wagenaar 2017

6.6 Cryostat wiring

The wiring in a multi-user cryostat is subject to multiple constraints: First of all, all wires together have a tight upper bound on the heat conductance they might add between any two different temperature plates. The heat load on the 3 K stage should remain below $\sim$ 1 W; while the heat load onto the mixing chamber should be below $\sim$ 10 μW. A wire with low heat conductance implies low electrical conductance wires or superconducting wires. The latter is usually only practical between plates that have a temperature lower than 4 K. The second constraint is the interference of signals between experiments. Therefore, using twisted pairs and never using the frame or shielding as return path is mandatory for low frequency signals.[38] Preferably every twisted pair should be shielded for electrical fields, while the twisting will minimize the magnetic field interferences. For high frequencies we prefer semirigid cabling as they feature minimal RF-leackage. At low temperatures (10 mK) the maximum frequency of thermal phonons and photons is about 200 MHz, while the RF-signal can be much higher in frequency. So avoiding RF-leakage, which heats the experiment due to electron-phonon coupling, and filtering the low frequency wiring with filters is essential.

[38] Low frequency means wavelengths much longer than electrical signal path.

#	conductor	insulator	shielding	use
1	phosphor-bronze	PTFE & graphite	CuNi braid	RT to MC; sensitive signals with $\ll 10$ MHz and $\ll 100$ µA
2a	copper	PTFE	CuNi braid	RT to 4K; coarse signals with $\ll 10$ MHz and ~ 1 mA
2b	NbTi in CuNi	PTFE	CuNi braid	4K to MC; coarse signals with $\ll 10$ MHz and ~ 1 mA
3a	copper	PTFE & graphite	CuNi braid	RT to 1K; SQUID signals with $\ll 10$ MHz and ~ 1 mA
3b	NbTi in CuNi	PTFE & graphite	CuNi braid	1K to MC; SQUID signals with $\ll 10$ MHz and ~ 1 mA
4a	Ag plated CuNi	PTFE	CuNi	RT to 4K; RF signals, $0 - 10$ GHz
4b	NbTi	PTFE	NbTi	4K to MC; RF signals, $0 - 10$ GHz
5a	Cu	-	-	RT to 50K; very high currents, max 100 A
5b	High Tc	-	-	50K to 4K; very high currents, max 100 A
5c	NbTi in CuNi	-	-	4K to 1K; very high currents, max 100 A

THE WIRING summarized in the table above suits the current purposes of the multi-user cryostat very well. The wires $1 - 3$ are used in 24-wire assemblies with multipin connectors on each end. To sum up, we used 6×12 plus 4×1 twisted pairs of type 1, 5×12 twisted pairs of type 2, three 8-wire cables with types 1 and 3 for SQUID-control, 4 semirigids of type 4, and one set of type 5, which leads to a total amount of about 300 shielded conductors going from room temperature (RT) to the mixing chamber (MC).[39]

[39] The mixing chamber can reach a temperature below 10 mK.

AT LOW TEMPERATURES we use a custom made 3×12 pins female connector. Inside the connector each stroke of 3 pins are separately shielded, and one of the three pins is connected to the shielding. This way, the connector itself is a small break-out box to which various cables can be plugged in, see Fig. 6.11.

Figure 6.11: 3×12 pins connector for use at low temperatures. The left column of pins is connected to the connector housing to provide a connection for the shielding of the plugged in cables.

6.7 *From cryostat to electronics*

IN A MULTI-USER ENVIRONMENT, colleagues will connect electronics that possibly interferes with another experiments. To minimize this interference while keeping all flexibility we developed break-out boxes with thorough interference protection, see Fig. 6.12. Starting from the cryostat we used a shielded cable with 12 shielded twisted pairs to connect the cabling from the cryostat to the break-out box that is mounted next to the the measurement electronics inside a 19" inch rack. The bundle of twisted pairs inside the cable ends

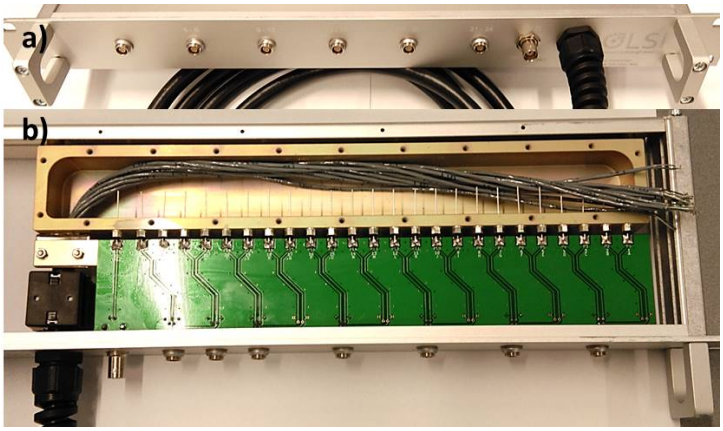

Figure 6.12: Breakout box as manufactured by LSI B.V. a) front panel with 6×4-pins LEMO connectors. b) Inside of the breakout box. The cabling inside the RF-shielded box have yet to be connected to the EMI feedthrough filters. This box has a frontpanel with 5×4- and 2×2-pins LEMO connectors. The single BNC connector, which is connected to the inside shielding of the black cable, can be used to measure noisy voltages between cryostat and 19" rack.

inside an RF-closed box. The wires only come out through pi-sections; a coaxial array of pi-filters[40] that filter from ~ 5 MHz and have a > 45 dB reduction from 100 MHz to at least 10 GHz. We have noticed that SQUIDs inside the cryostat regularly unlock upon some event outside the cryostat when cables of other nonSQUID equipment were connected to the cryostat *without* this breakout box, while this problem was solved *with* this breakout box. Note that this was the case even though the SQUID cabling was not connected to the breakout box.

Also, connecting commercial scientific instruments to wires that are inductively or even only capacitively coupled to the SQUID created large problems before, while this is now reduced to low frequency interferences only.[41]

[40] EMI Feedthrough Filters 1500pF *from* Tusonix

[41] Such as 50 Hz plus multiples, and switch-mode frequencies that some instruments like to broadcast.

6.8 Electronic infrastructure

But there is more that can be done to prevent unnecessary excess noise and interferences. The basic paradigm is: remove all potential noise sources and provide a preferred path for the remaining inevitable noise currents. How this can be done is schematically shown in Fig. 6.13.

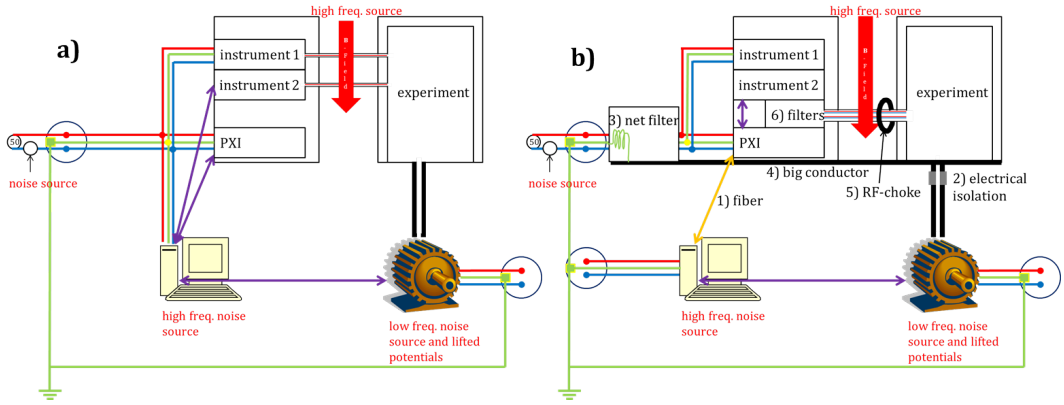

Figure 6.13: Simplified schematic of our set-up a) without and b) with action taken to prevent unnecessary noise. Precaution $1-3$ decouples the most obvious noise sources while $4, 5$ makes the remaining noise currents harmless. The break-out box (6) guards the input of the experiment in the cryostat and is discussed in the previous section.

Note that the clean part (the experiment and scientific instruments) is referenced to a potential at a single point. It is highly recommended to use the standard safety earth potential for safety reasons. Note that the precise potential does not matter for noise prevention as long as the frequencies of the reference potential, with respect to the surrounding potentials, are low enough, i.e. the wavelength should be much larger than the system size to avoid resonances due to its self-capacitance or capacitance to surroundings. To avoid such frequencies we placed a lossy coil between the reference point and the system (inside the net filter), thereby compromising < 10 µs peak voltage protection. It is not likely that these short peaks will cause injuries, however, see note 43.

Nowadays even scientific electronics uses digital processors and switch mode power supplies leading to signals at 50 Hz and (mainly odd) multiples, switch-mode signals in the 10 kHz - 5 MHz regime, and digital noise in the very and ultra high frequency regime ($30-3000$ MHz). Of course, for many applications we only need specific frequency bands, so everything else can be filtered. In our case, this is automatically done for all signals passing through the break-out box. Filtering also other parts of the remaining frequency regime[42] can prevent amplifiers from going into saturation. Moreover,

[42] Such as AC-coupling that many instruments provide.

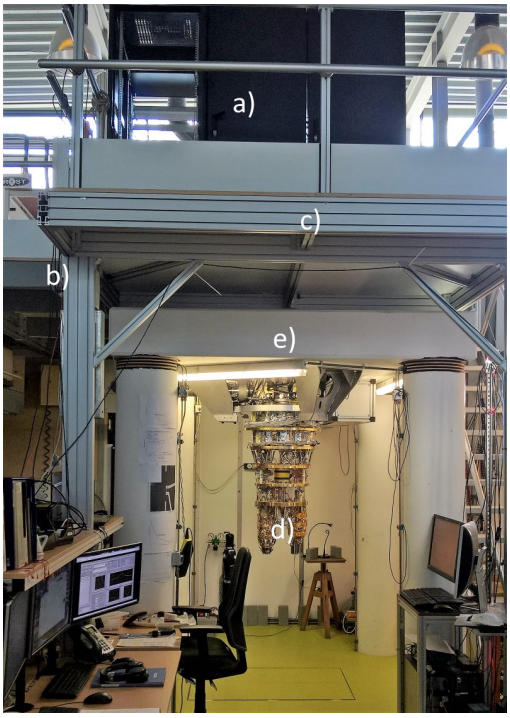

Figure 6.14: Cryostat setup. a) Three 19" instrument racks are connected with glassfibers (b) to the operator's computers. c) The platform is covered with metal plates on top that are welded to each other. The cryostat and 19" racks are connected to this big conductor with thick copper leads and metal supports. d) The experiment(s) hanging below the (open) cryostat. e) A heavy concrete 'temple' on which the cryostat is hanging. The temple stands on a different foundation than the building to avoid acoustic interference.

as a rule of thumb, it is usually best to pre-amplify signals going into or attenuate signals coming out of commercial scientific instruments such that they can make optimal use of their dynamical range at their input *and* output.

To MAKE SURE that every user adapts to this way of working, we needed to construct it in such a way that it takes effort to *not* work this way.[43] Therefore we lifted all 19" racks that contain measurement instruments to a higher floor, see Fig. 6.14.

[43] Little did we know that scientists can be so desperate that they put effort in directly connecting the experiment to their computers, instead of using optical decoupling, and thereby possibly grilling their USB-controllers.